Check for updates

ADVANCED MATERIALS
www.advmat.de

3D Hydrogel Encapsulation Regulates Nephrogenesis in Kidney Organoids

*Bryan A. Nerger, Sumit Sinha, Nathan N. Lee, Maria Cheriyan, Pascal Bertsch, Christopher P. Johnson, L. Mahadevan, Joseph V. Bonventre, and David J. Mooney**

Stem cell-derived kidney organoids contain nephron segments that recapitulate morphological and functional aspects of the human kidney. However, directed differentiation protocols for kidney organoids are largely conducted using biochemical signals to control differentiation. Here, the hypothesis that mechanical signals regulate nephrogenesis is investigated in 3D culture by encapsulating kidney organoids within viscoelastic alginate hydrogels with varying rates of stress relaxation. Tubular nephron segments are significantly more convoluted in kidney organoids differentiated in encapsulating hydrogels when compared with those in suspension culture. Hydrogel viscoelasticity regulates the spatial distribution of nephron segments within the differentiating kidney organoids. Consistent with these observations, a particle-based computational model predicts that the extent of deformation of the hydrogel–organoid interface regulates the morphology of nephron segments. Elevated extracellular calcium levels in the culture medium, which can be impacted by the hydrogels, decrease the glomerulus-to-tubule ratio of nephron segments. These findings reveal that hydrogel encapsulation regulates nephron patterning and morphology and suggest that the mechanical microenvironment is an important design variable for kidney regenerative medicine.

1. Introduction

Nephrons form the functional unit of the kidney and are responsible for filtering blood and processing the filtrate. While tubular epithelial cells in nephrons can proliferate to repair damage,[1–3] the human postnatal kidney has a limited regenerative capacity and cannot produce new nephrons. Nephron loss due to acute kidney injury or chronic kidney disease is therefore irreversible and often results in renal failure. Stem cell-derived human kidney organoids have emerged as a promising strategy for studying human kidney disease as well as regenerating and repairing nephrons in vivo. Directed differentiation of human pluripotent stem cells (hPSCs) generates kidney organoids that contain nephron-like structures with podocytes, proximal and distal tubules, and loops of Henle.[4–6] However, kidney organoids do not recapitulate the cellular complexity of mature nephrons in vivo; rather, they resemble first[4] or second[7] trimester human fetal kidneys. These limitations, along with evidence that mechanical signals impact kidney organoid differentiation,[7–11] suggest that biochemical signals alone are insufficient to generate mature nephrons in culture.

Extracellular matrix (ECM) mechanical properties such as stiffness and viscoelasticity regulate cell behaviors, including proliferation,[12] differentiation,[13] and migration,[14] that drive nephrogenesis. We therefore hypothesize that 3D encapsulation of differentiating kidney organoids will affect the cellular

B. A. Nerger, S. Sinha, L. Mahadevan, D. J. Mooney
John A. Paulson School of Engineering and Applied Sciences
Harvard University
Cambridge, MA 02138, USA
E-mail: mooneyd@seas.harvard.edu

B. A. Nerger, C. P. Johnson, D. J. Mooney
Wyss Institute for Biologically Inspired Engineering
Harvard University
Boston, MA 02115, USA

S. Sinha
Department of Data Science
Dana-Farber Cancer Institute
Boston, MA 02215, USA

N. N. Lee, J. V. Bonventre
Division of Renal Medicine
Department of Medicine
Brigham and Women's Hospital
Harvard Medical School
Boston, MA 02115, USA

M. Cheriyan
Harvard College
Harvard University
Cambridge, MA 02138, USA

P. Bertsch
Radboud University Medical Center
Department of Dentistry – Regenerative Biomaterials
Radboud Institute for Molecular Life Sciences
Nijmegen 6525 EX, Netherlands

L. Mahadevan
Department of Physics
Harvard University
Cambridge, MA 02138, USA

The ORCID identification number(s) for the author(s) of this article can be found under https://doi.org/10.1002/adma.202308325

DOI: 10.1002/adma.202308325

 © 2024 Wiley-VCH GmbH

organization of nephrons. 3D hydrogel encapsulation enables the presentation of mechanical signals to cells in a physiologically relevant microenvironment[15] and significantly impacts embryonic stem cell differentiation when compared with 2D culture.[16,17] Although Matrigel and type I collagen hydrogels are commonly used for encapsulation of kidney cells,[18–21] animal-derived ECMs have a limited stiffness range. Moreover, these materials can have lot-to-lot variability,[22] poorly defined compositions,[22] and risks from immunogen and pathogen transfer. Synthetic ECMs such as polyacrylamide (PA)[7] and polyethylene glycol (PEG)[23–25] have been used as xenogenic-free alternatives due to their defined composition, tunable mechanical properties, and ready chemical modification. However, precursors for PA hydrogels are toxic, precluding 3D encapsulation, while PEG hydrogels are largely covalently crosslinked, which generates elastic behavior that does not capture the time-dependent viscoelastic properties of the ECM.[26] PEG hydrogels with dynamic covalent crosslinks are viscoelastic, but these materials cannot currently reproduce the extent of stress relaxation of ECM hydrogels such as Matrigel.[27]

The role of mechanical signals in nephrogenesis also remains unclear because the mechanical properties of the nephrogenic niche in the developing kidney are unknown. The impact of ECM mechanics on nephrogenesis has largely been explored using very soft (≈0.1–1 kPa) elastic materials in 2D or 2.5D microenvironments[7,11] that do not account for the viscoelastic properties of tissues and ECM. Recently, soft viscoelastic hydrogels have been added on top of kidney organoids grown on a transwell membrane,[10] but the rate of hydrogel relaxation was at least an order of magnitude larger relative to the postnatal pig kidney.[28] 3D differentiation of kidney organoids in synthetic peptide hydrogels[9] or kidney decellularized ECM/Matrigel[29] improves differentiation, but it is unclear how mechanics of these materials compare to the developing kidney. Identifying biomaterials that recapitulate the mechanical environment of the developing kidney and support kidney organoid differentiation in 3D culture will enable further investigation of how mechanics regulate nephrogenesis.

Here, we use ionically crosslinked alginate hydrogels to investigate how stiffness and viscoelasticity influence 3D differentiation of encapsulated human kidney organoids. Both the stiffness and the viscoelasticity of the alginate hydrogels are designed to approximate the mechanical properties of the developing embryonic mouse kidney. In contrast to native ECM, alginate hydrogels cannot be degraded by mammalian cells[30] and enable viscoelasticity to be tuned independently of stiffness and ligand density.[26] Moreover, ionically crosslinked alginate hydrogels can approximate the fast rates of stress relaxation observed in the developing kidney while remaining stable in culture over several weeks. Encapsulation of differentiating kidney organoids in alginate reveals that matrix mechanics regulate nephron morphology and patterning and informs design principles for engineering biomaterials for kidney regenerative medicine.

L. Mahadevan
Department of Organismic and Evolutionary Biology
Harvard University
Cambridge, MA 02138, USA
J. V. Bonventre
Division of Engineering in Medicine
Department of Medicine
Brigham and Women's Hospital
Harvard Medical School
Boston, MA 02115, USA

2. Results

2.1. Alginate Hydrogels Support 3D Differentiation of Kidney Organoids

We began by generating kidney organoids from human embryonic stem cells (hESCs; H9 line) in 3D suspension culture. Using a directed differentiation approach modified from a previously developed protocol,[6] embryoid bodies were differentiated for 21 d. The resulting kidney organoids contained proximal tubules (positively stained with *lotus tetragonolobus* lectin; LTL), podocytes (positively stained for podocalyxin; PODXL), and distal tubules (positively stained for E-cadherin; ECAD) (**Figure 1a,b**). Nephron segments were organized with proper proximal-to-distal patterning (Figure 1b) and contained additional markers for distal tubules (Figure S1, Supporting Information), basement membrane (Figure S2, Supporting Information), and vasculature (Figure S3, Supporting Information). Regions of high mitochondrial density in tubular nephron segments and cell membrane folds between podocyte-like cells were visible with transmission electron microscopy (TEM) (Figure S4, Supporting Information).

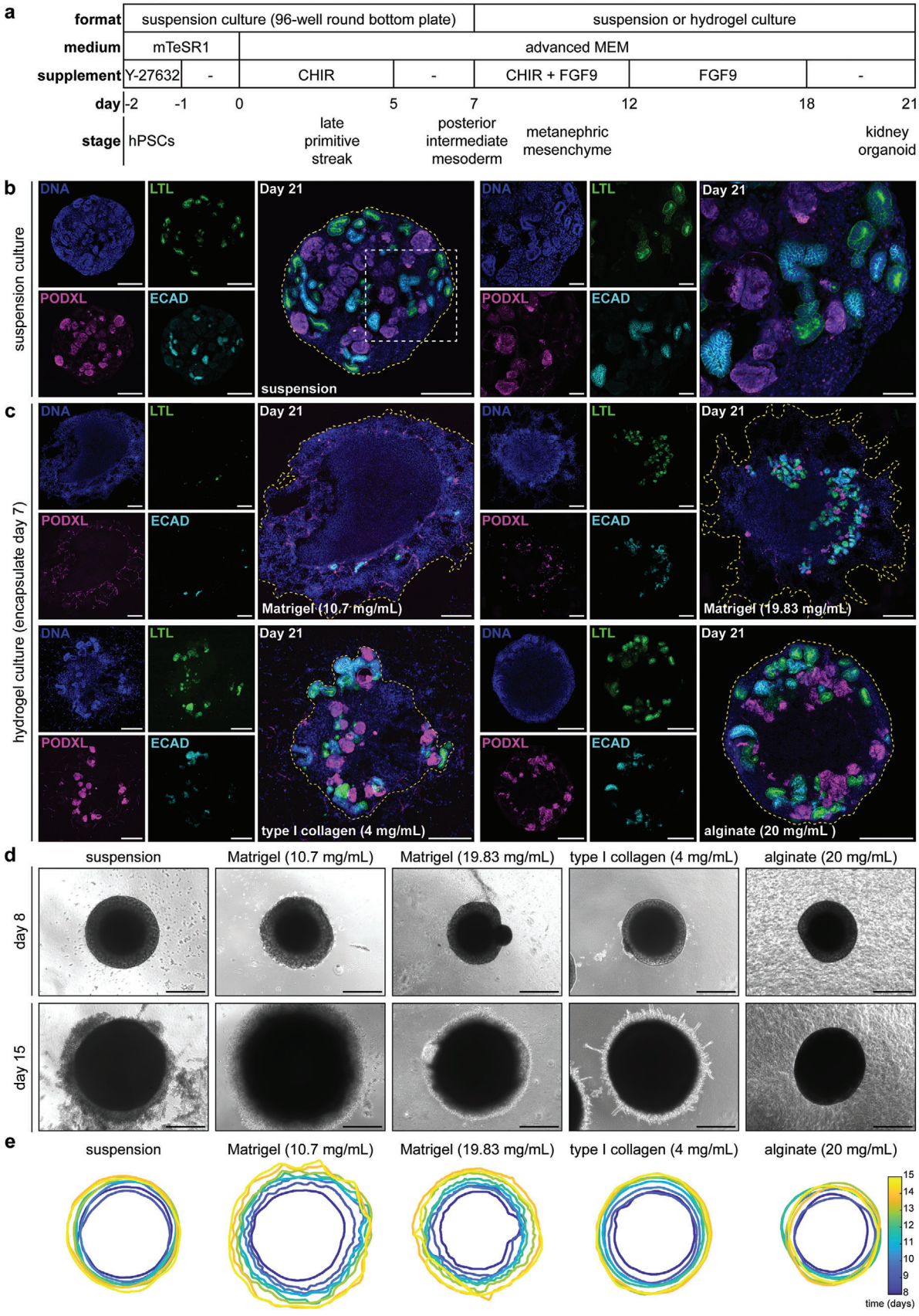
To understand the impact of physical confinement on nephrogenesis, organoids were encapsulated on day 7 of the differentiation protocol into Matrigel, type I collagen, or alginate hydrogels (Figure 1c). Sporadic differentiation was observed in Matrigel and type I collagen hydrogels, which is likely due, in part, to cell migration away from organoids during differentiation and differences in cell proliferation (Figure 1c–e and Figure S5, Supporting Information). The resulting organoids contained markers for renal stroma and off-target cell populations (Figure S6, Supporting Information). In contrast, organoids encapsulated in alginate hydrogels differentiated without significant cell migration (Figure 1d,e and Figures S5 and S7, Supporting Information), and all major nephron segments were present after 21 d of differentiation (Figure 1c and Figures S1–S4, Supporting Information). In the absence of physical confinement, organoids in suspension culture extruded cells that had persistent elevated levels of intracellular calcium (Ca^{2+}) (Figure S8, Supporting Information). These data show that nondegradable alginate hydrogels can provide a 3D mechanical environment that supports kidney organoid differentiation.

2.2. Alginate Hydrogels Approximate the Mechanical Properties of the Mouse Embryonic Kidney

The mechanical properties of the embryonic mouse metanephric mesenchyme, within which nephrons develop, were characterized with atomic force microscopy (AFM) to identify the range of stiffness and viscoelasticity relevant for nephrogenesis. To visualize the mesenchyme in unfixed tissue, sections of embryonic kidneys (E15-E17) from SIX2Cre(+)EGFP mice were analyzed, wherein the population of SIX2-expressing nephron progenitor cells (NPCs) are EGFP positive (**Figure2a**).[31] In terms

© 2024 Wiley-VCH GmbH

15214095, 2024, 14, Downloaded from https://onlinelibrary.wiley.com/doi/10.1002/adma.202308325 by Seoul National University, Wiley Online Library on [14/05/2024]. See the Terms and Conditions (https://onlinelibrary.wiley.com/terms-and-conditions) on Wiley Online Library for rules of use; OA articles are governed by the applicable Creative Commons License



© 2024 Wiley-VCH GmbH

15214095, 2024, 14, Downloaded from https://onlinelibrary.wiley.com/doi/10.1002/adma.202308325 by Seoul National University, Wiley Online Library on [14/05/2024]. See the Terms and Conditions (https://onlinelibrary.wiley.com/terms-and-conditions) on Wiley Online Library for rules of use; OA articles are governed by the applicable Creative Commons License

of stiffness, the region of the developing kidney that contains SIX2-expressing NPCs had an average Young's modulus (E) of ≈0.88 kPa (Figure 2b). To evaluate viscoelasticity, the third time ($t_{1/3}$) of force relaxation upon indentation of the mesenchyme was quantified. Rapid relaxation with an average $t_{1/3}$ relaxation time of ≈9 s was observed (Figure 2b).

Alginate hydrogels with mechanical properties that varied around the measured properties of the metanephric mesenchyme were next developed. To control hydrogel viscoelasticity independently of stiffness or ligand density,[26] the concentration of Ca^{2+} crosslinker and alginate molecular weight were altered (Figure 2c). Soft alginate hydrogels ($E \approx 3$ kPa; $G' \approx 0.5$ kPa) were designed to approximate the stiffness of the mouse embryonic kidney, and stiff hydrogels ($E \approx 13$ kPa; $G' \approx 5$ kPa) were designed to be an order of magnitude stiffer (Figure 2d and Figure S9, Supporting Information). Viscoelastic gels with fast stress relaxation (fast) and slow stress relaxation (slow) were obtained by varying the molecular weight of alginate (Figure 2e and Figure S9, Supporting Information). Fast gels approximated the stress relaxation properties of the embryonic kidney at short timescales (<10 s) (Figure 2e,f), although the stress relaxation profiles of the gels and mouse embryonic kidneys deviated at longer times. These deviations may be due, in part, to differences in the bulk compression testing of hydrogels and local AFM analysis of the mouse embryonic kidney tissues.

2.3. 3D Encapsulation of Differentiating Kidney Organoids Affects Nephron Patterning and Morphology

To understand how stiffness and viscoelasticity impact nephrogenesis, kidney organoids were encapsulated on day 7 of differentiation into alginate hydrogels (**Figure 3**a). Because alginate does not have any cell-binding domains, arginine–glycine–aspartic acid (RGD) ligands were conjugated to the alginate to mediate integrin engagement. Quantification of the fraction of PODXL, LTL, and ECAD nephron segments revealed a shift in nephron patterning in encapsulated organoids (Figure 3b,c). Relative to suspension culture, the fraction of PODXL nephron segments decreased while LTL and ECAD markers for tubular nephron segments increased (Figure 3c). In encapsulated organoids, PODXL nephron segments decreased in size while the size of LTL and ECAD nephron segments remained unchanged (Figure S10, Supporting Information). The fraction of organoid cross-sectional area (Figure S11, Supporting Information) filled with nephron segments was significantly higher in stiff fast relaxing hydrogels relative to soft slow relaxing gels (Figure 3d). LTL and ECAD nephron segments were also found to have more convoluted geometries, as quantified by decreased circularity [Equation (1), Experimental Section], in encapsulated organoids relative to suspension culture (Figure 3e–g). Both the nephron patterning shift and the decreased circularity of nephron segments were observed in all alginate gel conditions, independent of the stiffness or viscoelasticity. However, based on the distribution of nephron segments observed in fluorescent images (Figure 3b), we hypothesized that organoids encapsulated in slow relaxing hydrogels had decreased nephron density relative to fast relaxing hydrogels. Quantification of the density of nephron segments as a function of radial position revealed that the spatial positioning of nephrons varied with hydrogel viscoelasticity as hypothesized (Figure S12, Supporting Information). Hydrogels with slow rates of stress relaxation resulted in a reduced fraction of nephron segments located along the inner edge and core of the organoids relative to hydrogels with fast stress relaxation (Figure S12, Supporting Information). Moreover, the radial position of the peak nephron density was significantly closer to the organoid perimeter in slow relaxing hydrogels (Figure S12, Supporting Information). Encapsulating organoids in alginate on day 0 of the differentiation protocol resulted in no differentiation, which is likely due to the loss of SIX2 and SALL1 transcription factor staining in cell nuclei (Figure S13, Supporting Information). Together, these data demonstrate that kidney organoid encapsulation in alginate hydrogels affects the circularity, spatial localization, and the glomerulus-to-tubule ratio of nephron segments.

We next sought to identify the mechanism by which nephron patterning and morphology were altered in encapsulated kidney organoids. To test if the increased LTL and ECAD segments in encapsulated organoids were a result of accelerated differentiation, the organoid suspension culture was extended to day 30. Extending organoid culture in suspension did not reproduce the nephron patterning shift observed when organoids were encapsulated (Figure S14, Supporting Information), suggesting that altered rates of differentiation in encapsulated kidney organoids are not driving changes in nephron patterning.

The role of RGD-mediated mechanical interactions was investigated next by differentiating kidney organoids in alginate hydrogels without RGD peptides (**Figure 4**a). Quantification of the fraction of nephron segments revealed a similar nephron patterning shift as observed with RGD-functionalized alginate, with reduced PODXL and increased LTL and ECAD nephron segments (Figure 4b and Figure S15, Supporting Information). In addition, similar trends were observed for the circularity of tubular nephron segments for organoids differentiated in gels without RGD (Figure 4c and Figure S15, Supporting Information). The density of nephron segments as a function of distance from the organoid perimeter followed the same trend as with RGD alginate, wherein nephron segments in slow relaxing gels were predominately located close to the perimeter of the organoid (Figures S15 and S16, Supporting Information). However, the differences in nephron density between fast and slow hydrogels

Figure 1. Alginate hydrogels support the differentiation of human kidney organoids in 3D culture. a) Directed differentiation protocol for the generation of kidney organoids from hESCs. b) Representative fluorescent images of kidney organoids differentiated in suspension culture showing markers for podocytes (PODXL), proximal tubules (LTL), and distal tubules (ECAD). Scale bars represent 200 µm (low magnification) and 50 µm (high magnification). c) Representative fluorescent images of kidney organoids encapsulated on day 7 of differentiation in alginate (stiff fast; see Figure 2), Matrigel, or type I collagen and cultured in these matrices for the last two weeks of differentiation. Scale bars represent 200 µm. d) Phase contrast images of kidney organoids on day 8 and day 15 of the differentiation protocol. Scale bars represent 500 µm. e) Outlines of the perimeter of kidney organoids on days 8 through 15 of the differentiation protocol. All fluorescent images except 1b (high magnification) represent a single optical slice of a 50-µm-thick organoid cryosection. The dashed yellow outlines denote the perimeter of the organoids.

© 2024 Wiley-VCH GmbH

15214095, 2024, 14, Downloaded from https://onlinelibrary.wiley.com/doi/10.1002/adma.202308325 by Seoul National University, Wiley Online Library on [14/05/2024]. See the Terms and Conditions (https://onlinelibrary.wiley.com/terms-and-conditions) on Wiley Online Library for rules of use; OA articles are governed by the applicable Creative Commons License

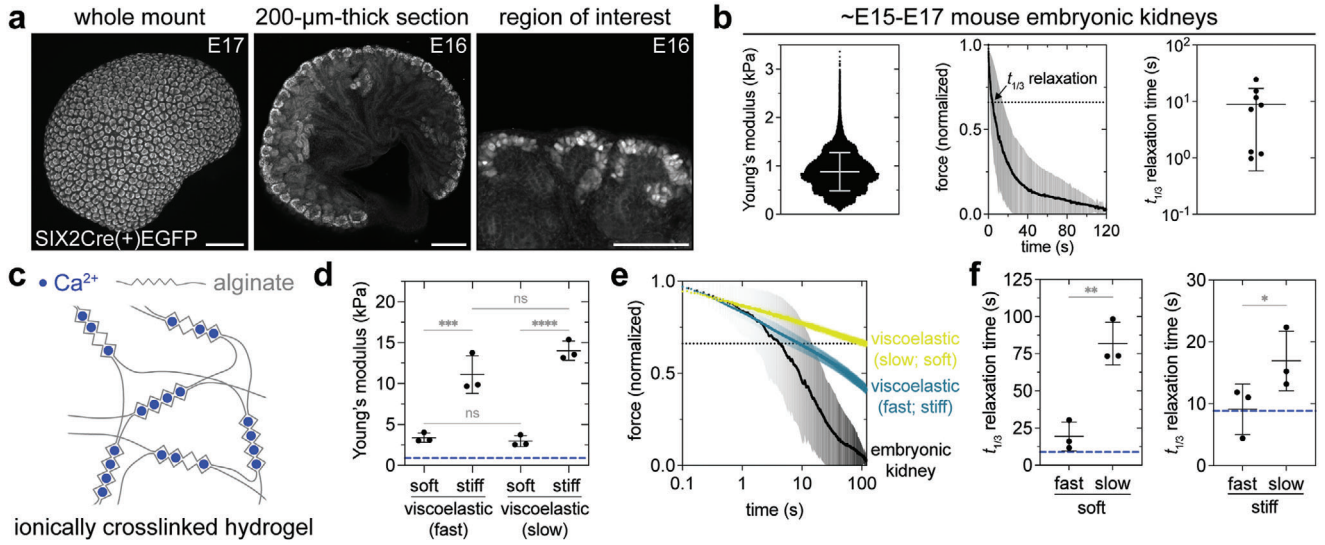


Figure 2. Alginate hydrogels approximate the soft viscoelastic mechanical properties of the metanephric mesenchyme in the mouse embryonic kidney. a) Representative fluorescent images of SIX2Cre(+)EGFP mouse embryonic kidneys. Scale bars represent 500 µm (left), 250 µm (middle), and 100 µm (right). b) Young's modulus, force relaxation, and $t_{1/3}$ relaxation time of force relaxation of embryonic mouse kidneys measured with AFM. Young's modulus data are shown as individual measurements (n = 81 622) acquired from n = 7 area scans (25 µm^2) of n = 7 embryonic kidney tissues. Force relaxation and $t_{1/3}$ relaxation time data represent n = 8 measurements over n = 3 embryonic kidney tissues. Aggregate data of E15-E17 kidneys are shown. c) Schematic of viscoelastic alginate hydrogel crosslinked with Ca^{2+} ions. d) Young's modulus and e) normalized force relaxation of alginate hydrogels relative to E15–E17 mouse embryonic kidney tissues. f) $t_{1/3}$ time of force relaxation of alginate hydrogels. The blue dashed lines represent the d) average Young's modulus or f) $t_{1/3}$ relaxation time of E15–E17 mouse embryonic kidney tissue. Statistical comparisons were performed using an ordinary one-way ANOVA (d) or a one-tailed Student's t-test (f) with n = 3 gels per condition. Data represent mean ± standard deviation (SD). *$p \leq$ 0.05, **$p \leq$ 0.01, ***$p \leq$ 0.001, ****$p \leq$ 0.0001, and ns, not significant.

were no longer significant, which suggests that RGD-mediated mechanical interactions may impact the effect of viscoelasticity on nephron density within the organoids. To further explore the mechanical interactions between kidney organoids and alginate hydrogels with and without RGD, organoids were stained for the mechanosensitive proteins phosphorylated focal adhesion kinase (pFAK) and yes-associated protein 1 (YAP) (Figure 4d). pFAK puncta were only observed around the perimeter of organoids encapsulated in alginate hydrogels with RGD (Figure 4d). Consistent with the culture of epithelial spheroids in viscoelastic hydrogels,[14] YAP was located in the cytoplasm of cells. Cytoplasmic localization of YAP is likely due to the high cell density, which is known to increase the fraction of cytoplasmic YAP.[34] These results suggest limited direct mechanical engagement through integrins between the organoid and the hydrogel and that encapsulation itself might be driving changes in nephron morphology.

Next, we investigated how encapsulation in viscoelastic hydrogels contributes to the observed changes in the morphology of tubular nephron segments. Kidney organoids were first differentiated in 2D on top of alginate hydrogels (**Figure 5a**), and the glomerulus-to-tubule patterning of the nephron segments was assessed (Figure 5b). Organoids differentiated in 2D on top of alginate hydrogels showed a similar shift in the glomerulus-to-tubule ratio as observed in 3D hydrogel culture (Figure 5c,d), which was independent of the hydrogel mechanical properties (Figure S17, Supporting Information). However, we did not observe any differences in the morphology of tubular LTL or ECAD nephron segments (Figure 5e). These results suggest that 3D encapsulation drives changes in nephron morphology while agents released from the gels into the culture medium may be responsible for the glomerulus-to-tubule patterning shift.

2.4. Ca^{2+} Release from Alginate Hydrogels Decreases the Ratio of Glomerulus-to-Tubule Nephron Segments

We next investigated how alginate hydrogels impact culture medium in the absence of cells. Ca^{2+} used to crosslink alginate hydrogels can be lost over time due to competition between Ca^{2+} and Na^+ at guluronic crosslink sites (**Figure 6a**).[35] To assess how Ca^{2+} loss from alginate hydrogels impacts culture medium, we immersed hydrogels in culture medium and performed medium changes comparable to the differentiation experiments with kidney organoids (Figure 6b). We observed that Ca^{2+} levels in the medium first increased and then gradually returned to normal levels as the medium was changed (Figure 6c). As expected, changes in the Ca^{2+} levels in the culture medium were most substantial for stiffer gels, which contain a higher concentration of Ca^{2+} for ionic crosslinking.

In addition to elevated Ca^{2+} in the culture medium, uncrosslinked alginate can be released from immersed hydrogels gels initially, and the loss of Ca^{2+} from the hydrogels over time could lead to further dissolution of alginate chains. We hypothesized that these changes would increase the osmolality of the culture medium. Analysis of culture medium conditioned with alginate hydrogels revealed elevated osmolality at the beginning and end of the experiment (Figure 6d). Consistent with these data, we observed a decrease in the Young's modulus and an increase in

© 2024 Wiley-VCH GmbH

15214095, 2024, 14, Downloaded from https://onlinelibrary.wiley.com/doi/10.1002/adma.202308325 by Seoul National University, Wiley Online Library on [14/05/2024]. See the Terms and Conditions (https://onlinelibrary.wiley.com/terms-and-conditions) on Wiley Online Library for rules of use; OA articles are governed by the applicable Creative Commons License

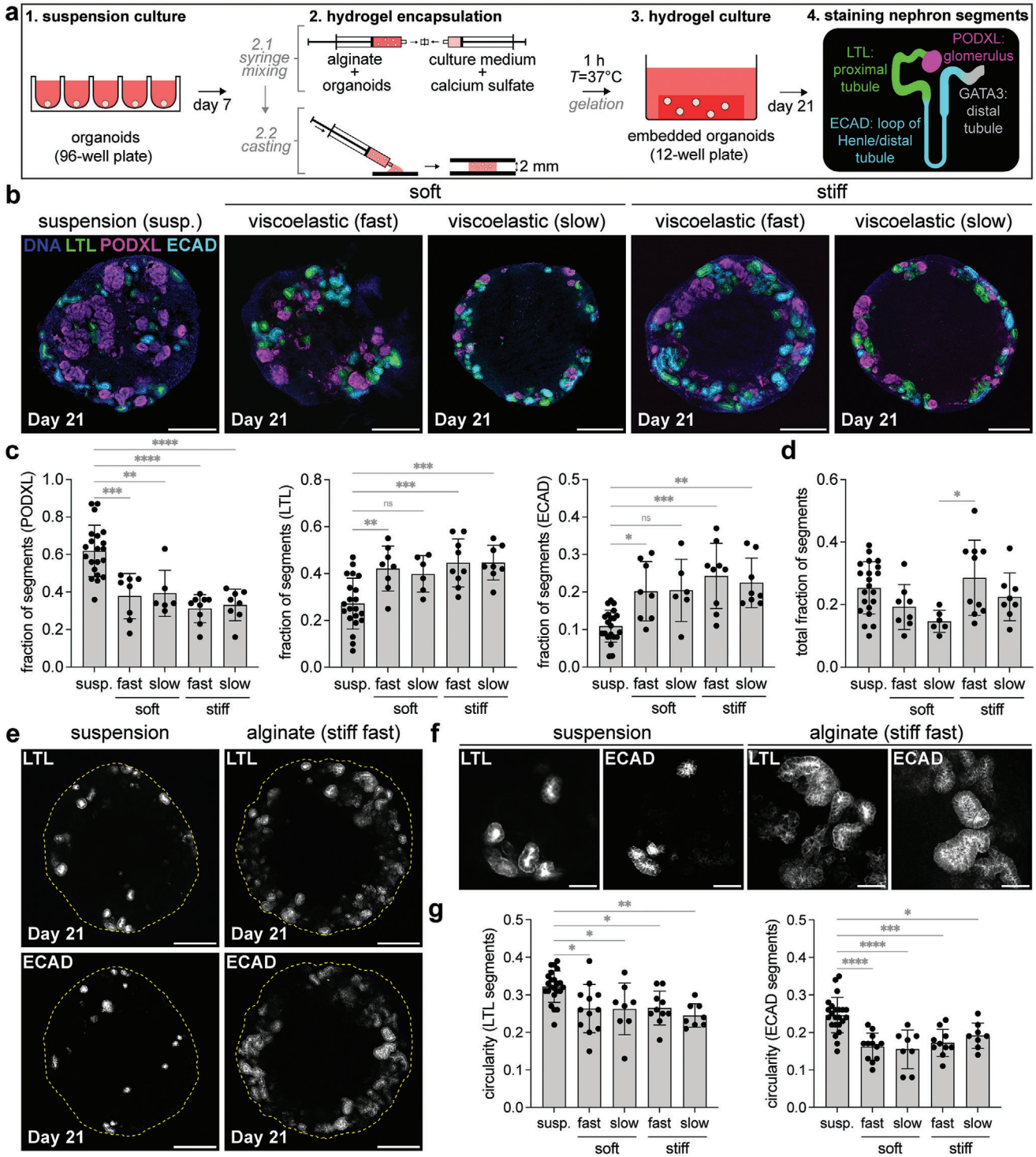


Figure 3. 3D differentiation of kidney organoids in alginate hydrogels affects nephron patterning and morphology. a) Schematic of kidney organoid embedding and post-fixation analysis. GATA3 is used here to denote distal tubules, but it is also expressed by mesangial cells in developing glomeruli.[32] Nephron schematic inspired by Rennke and Denker.[33] b) Representative fluorescent images of kidney organoids differentiated in suspension or encapsulated on day 7 and differentiated in alginate hydrogels. Scale bars represent 200 µm. c) Fraction of PODXL, LTL, and ECAD nephron segments in organoids. d) Total fraction of organoid cross-sectional area that contains any nephron segment. Representative e) low-magnification and f) high-magnification fluorescent images of LTL and ECAD nephron segments for organoids differentiated in suspension (left) or a stiff fast alginate hydrogel (right). Dashed yellow outlines denote the perimeter of the organoids. Scale bars represent 200 or 50 µm (high magnification). g) Circularity of LTL (left) or ECAD (right) segments in kidney organoids differentiated in suspension or in alginate hydrogels. Statistical comparisons were performed using an ordinary one-way ANOVA. $n = 21$, 9, 6, 9, and 8 organoids per condition (c, d) or $n = 23$, 12, 8, 10, and 8 organoids per condition (g). Data represent mean ± SD. *$p \leq 0.05$, **$p \leq 0.01$, ***$p \leq 0.001$, ****$p \leq 0.0001$, and ns, not significant.

© 2024 Wiley-VCH GmbH

15214095, 2024, 14, Downloaded from https://onlinelibrary.wiley.com/doi/10.1002/adma.202308325 by Seoul National University, Wiley Online Library on [14/05/2024]. See the Terms and Conditions (https://onlinelibrary.wiley.com/terms-and-conditions) on Wiley Online Library for rules of use; OA articles are governed by the applicable Creative Commons License

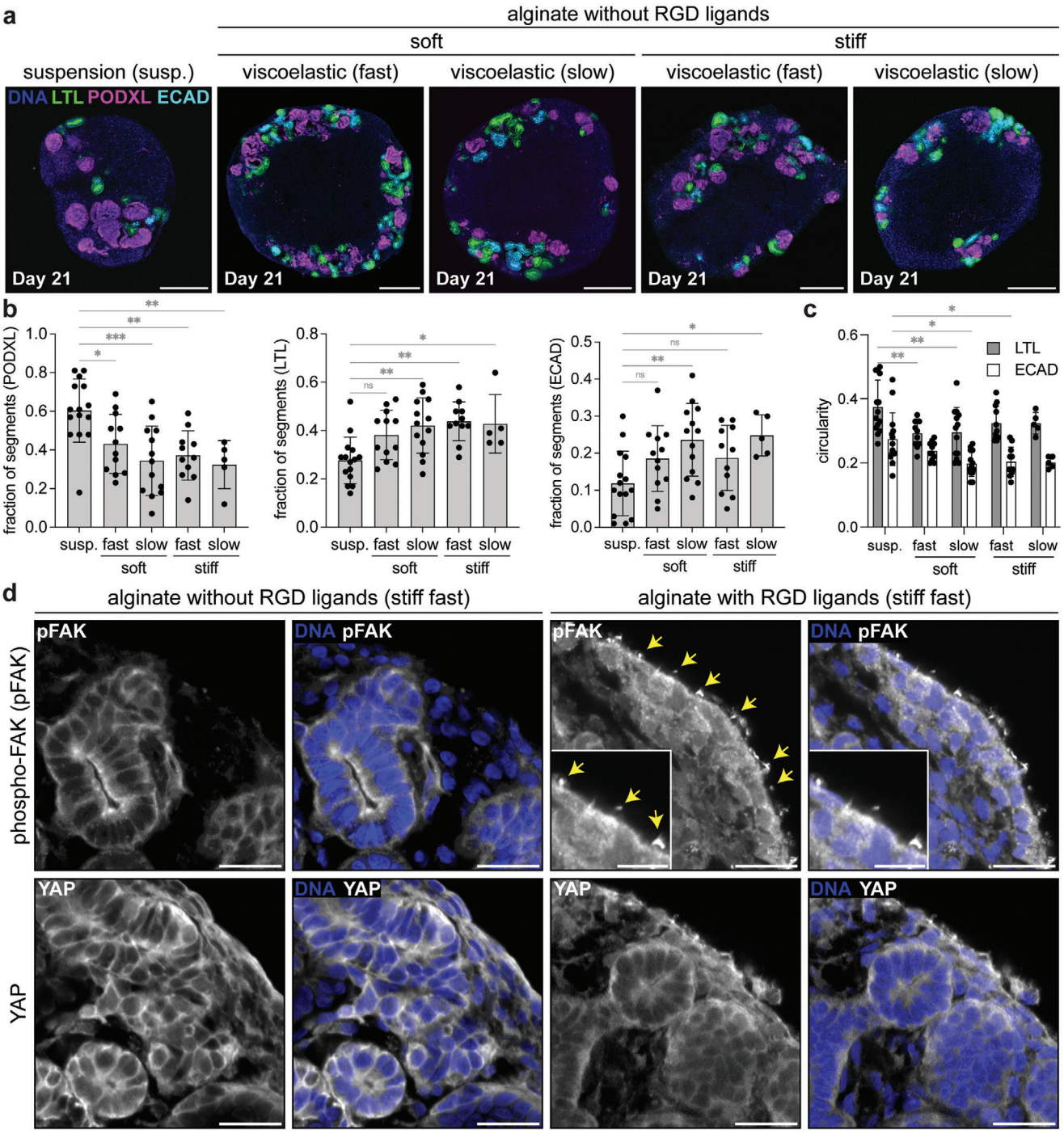


Figure 4. Nephron patterning and morphology are independent of RGD binding domains in alginate hydrogels. a) Representative fluorescent images of kidney organoids differentiated in suspension or in alginate hydrogels without RGD binding domains. Scale bars represent 200 µm. b) Fraction of PODXL, LTL, and ECAD nephron segments in kidney organoids. c) Circularity of LTL (gray) or ECAD (white) nephron segments in kidney organoids differentiated in suspension or in alginate hydrogels without RGD binding domains. d) Representative fluorescent images of pFAK and YAP in kidney organoids differentiated in stiff fast alginate hydrogels without RGD (left) and with RGD (right). Scale bars represent 25 or 12.5 µm for insets. Statistical comparisons were performed using an ordinary one-way ANOVA. n = 15, 12, 13, 11, and 5 organoids per condition (b) or n = 14, 11, 13, 11, and 5 organoids per condition (c). Data represent mean ± SD. *$p \leq 0.05$, **$p \leq 0.01$, ***$p \leq 0.001$, and ns, not significant.

© 2024 Wiley-VCH GmbH

15214095, 2024, 14, Downloaded from https://onlinelibrary.wiley.com/doi/10.1002/adma.202308325 by Seoul National University, Wiley Online Library on [14/05/2024]. See the Terms and Conditions (https://onlinelibrary.wiley.com/terms-and-conditions) on Wiley Online Library for rules of use; OA articles are governed by the applicable Creative Commons License

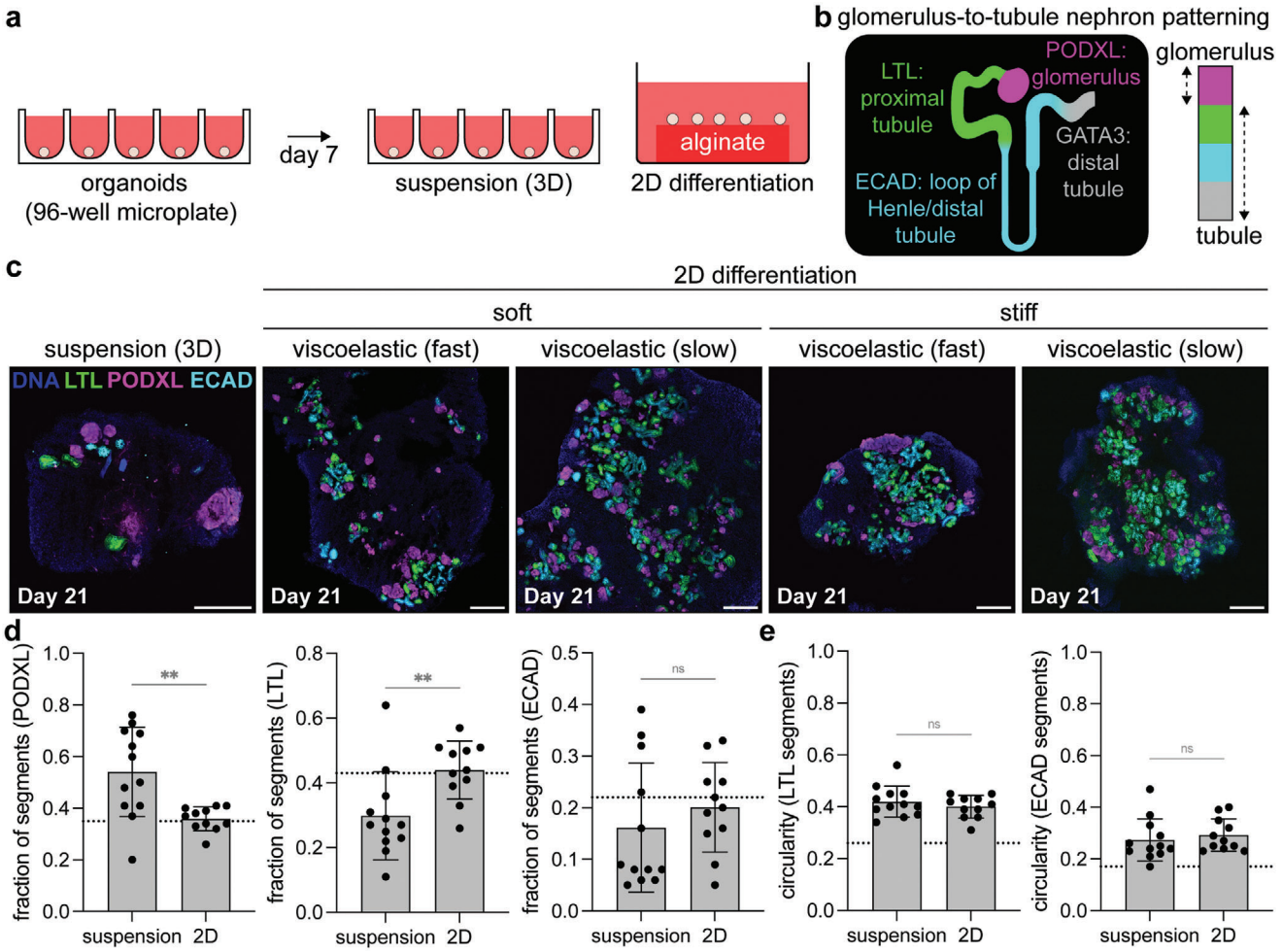


Figure 5. 2D differentiation alters the glomerulus-to-tubule ratio without affecting the morphology of tubular nephron segments. Schematic of a) differentiation of kidney organoids in 3D suspension culture or in 2D on top of alginate hydrogels and of b) nephron patterning. Schematic of nephron inspired by Rennke and Denker.[33] c) Representative fluorescent images of kidney organoids differentiated on top of RGD-functionalized alginate hydrogels. Scale bars represent 200 µm. d) Fraction of PODXL, LTL, and ECAD nephron segments in kidney organoids. 2D represents combined analysis for organoids differentiated on all four types of alginate hydrogels. e) Circularity of LTL (left) and ECAD (right) nephron segments. Dotted lines represent the average fraction of nephron segments (d) or circularity (e) for kidney organoids differentiated in 3D within alginate hydrogels. All fluorescent images represent a single optical slice of a 50-µm-thick organoid cryosection. Statistical comparisons were performed using a two-tailed Student's *t*-test. $n = 12$ and 11 organoids per condition (d, e). Data represent mean ± SD. $^{**}p \leq 0.01$ and ns, not significant.

the relaxation time of stiff alginate hydrogels immersed in culture medium (Figure S18, Supporting Information). The relaxation time of soft hydrogels also increased while the Young's modulus remained stable.

To understand if elevated extracellular Ca^{2+} could affect differentiation independent of the alginate hydrogel, kidney organoids were differentiated in suspension culture using medium with elevated levels of Ca^{2+} (Figure 6e). The Ca^{2+} concentration in culture medium was increased to the highest measured Ca^{2+} concentration (≈6×10^{-3} M) (Figure 6f) in an equilibrium process, which maintained the same osmolality as the control medium (Figure 6g). Analysis of kidney organoids after 21 d of differentiation revealed that all major nephron segments were present (Figure 6h). The same nephron patterning shift observed in 3D hydrogel culture was observed in suspension culture with elevated Ca^{2+} (Figure 6i), while the morphology of LTL and ECAD nephron segments was unchanged (Figure 6j). Nephron patterning of kidney organoids was weakly correlated with differentiation efficiency (Figure S19, Supporting Information), further supporting the role of Ca^{2+} in regulating nephron patterning as opposed to intrinsic batch-to-batch variability in nephron maturation and patterning.[36] These data suggest that elevated levels of extracellular Ca^{2+} in the culture medium drive changes in the glomerulus-to-tubule patterning of nephron segments.

The role of osmolality was next assessed by differentiating kidney organoids in culture medium with elevated osmolality. To increase osmolality, culture medium was supplemented with unpolymerized alginate (Figure S20, Supporting Information). Unexpectedly, culture medium supplemented with unpolymerized alginate prevented kidney organoid differentiation (Figure S20, Supporting Information). Elevating FGF9 levels to 50 ng mL^{-1} and reducing the culture time in elevated osmolality medium

© 2024 Wiley-VCH GmbH

15214095, 2024, 14, Downloaded from https://onlinelibrary.wiley.com/doi/10.1002/adma.202308325 by Seoul National University, Wiley Online Library on [14/05/2024]. See the Terms and Conditions (https://onlinelibrary.wiley.com/terms-and-conditions) on Wiley Online Library for rules of use; OA articles are governed by the applicable Creative Commons License

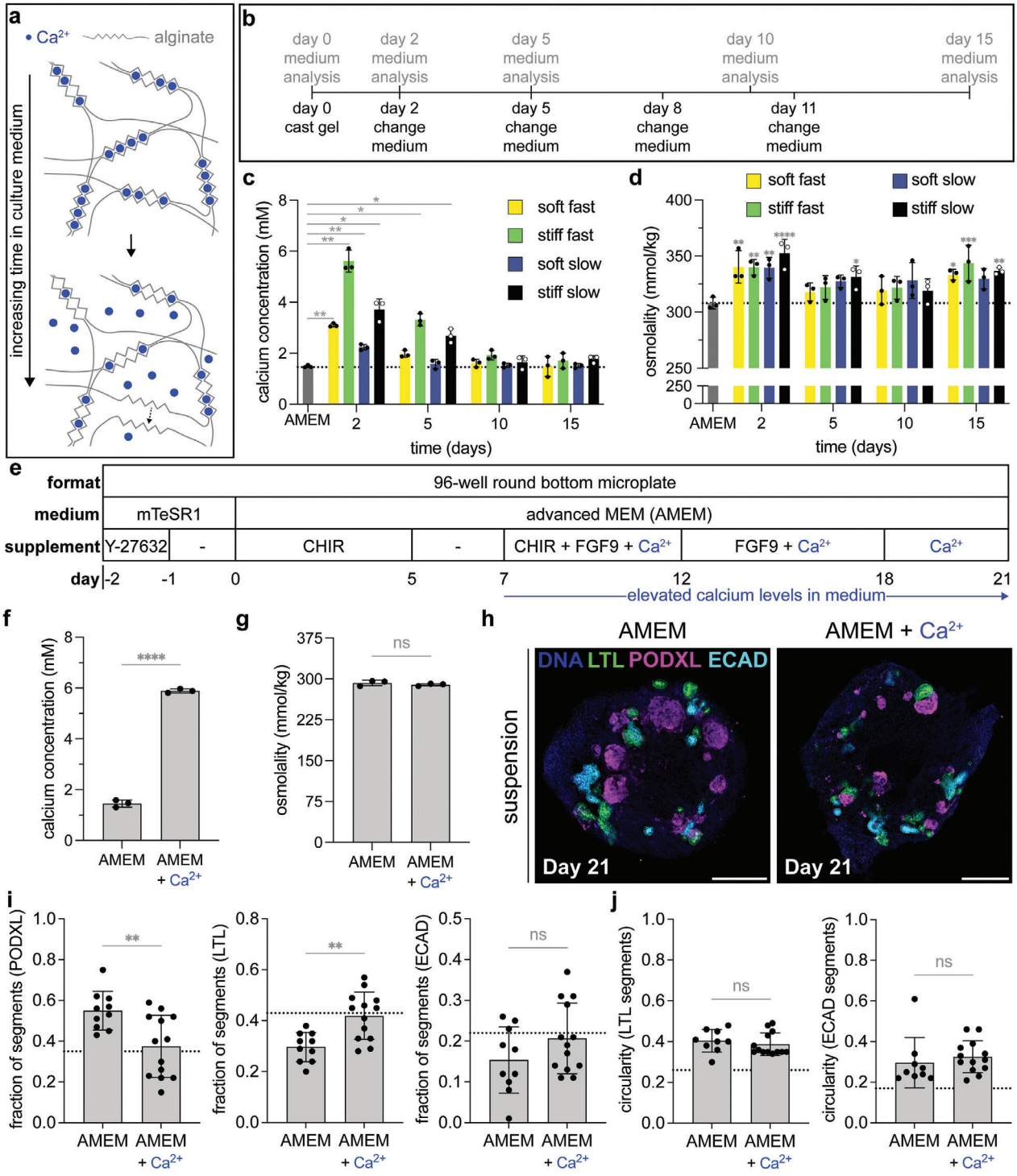


Figure 6. Elevated levels of extracellular Ca^{2+} affect the ratio of glomerular-to-tubular nephron segments. a) Schematic of alginate hydrogel in cell culture medium. b) Experimental timeline for medium changes and analysis. c) Ca^{2+} concentration and d) osmolality for culture medium conditioned with alginate hydrogels. Dotted lines represent average values for AMEM. e) Experimental timeline for the addition of Ca^{2+} to culture medium during kidney organoid differentiation. f) Ca^{2+} concentration and g) osmolality in medium with and without the addition of Ca^{2+}. h) Representative fluorescent images of kidney organoids differentiated in medium with and without the addition of Ca^{2+}. Scale bars represent 200 µm. i) Fraction of PODXL, LTL, and ECAD nephron segments in kidney organoids. j) Circularity of LTL (left) and ECAD (right) nephron segments. Dotted lines represent the average fraction of (i) nephron segments or (j) circularity for kidney organoids differentiated in 3D within alginate hydrogels. Statistical comparisons were performed using an ordinary two-way ANOVA (c, d) or a two-tailed Student's *t*-test (f, g, i, and j). $n = 3$ medium samples per condition (c, d, f, and g) or 10 and 13 organoids per condition (i) and 9 and 13 organoids per condition (j). Data represent mean ± SD. $^{*}p \leq 0.05$, $^{**}p \leq 0.01$, $^{***}p \leq 0.001$, $^{****}p \leq 0.0001$, and ns, not significant.

© 2024 Wiley-VCH GmbH

15214095, 2024, 14, Downloaded from https://onlinelibrary.wiley.com/doi/10.1002/adma.202308325 by Seoul National University, Wiley Online Library on [14/05/2024]. See the Terms and Conditions (https://onlinelibrary.wiley.com/terms-and-conditions) on Wiley Online Library for rules of use; OA articles are governed by the applicable Creative Commons License

enabled normal kidney organoid differentiation despite the presence of unpolymerized alginate and without any impact on nephron patterning (Figure S20, Supporting Information). Consistent with these findings, adjustment of osmolality using D-mannitol did not affect nephron patterning in kidney organoids (Figure S20, Supporting Information).

2.5. Deformation of the Hydrogel–Organoid Interface Regulates Nephron Morphology

We next sought to understand how 3D encapsulation of differentiating kidney organoids affects the morphology of nephron segments. To obtain a first principle-based perspective, we developed a particle-based computational model of nephrogenesis (Supporting Information) for kidney organoids encapsulated in hydrogels with different extents of deformation (**Figure 7a**). We modeled viscoelastic hydrogels with fast rates of stress relaxation as materials that experience larger deformations relative to hydrogels with slow rates of stress relaxation.

Consistent with experiments using alginate hydrogels with covalent norbornene–tetrazine (Nb-Tz) crosslinks (Figures S21 and S22, Supporting Information), simulations predicted that encapsulation of the differentiating kidney organoid in an elastic material with minimal deformation inhibits the formation of nephron segments (Figure 7b). Simulations also predicted that encapsulation in nondegradable materials generates nephron segments with a more convoluted geometry (Figure 7c), which is similar to experiments (Figure 7d). Unexpectedly, simulations predicted that differences in the length of nephron segments result from encapsulation in hydrogels with different extents of deformation (Figure 7e,f). We experimentally tested this prediction and observed differences in the length of proximal tubules in kidney organoids encapsulated in hydrogels (Figure 7g). However, no differences in the length of distal tubules were observed for kidney organoids encapsulated in hydrogels (Figure 7g). Simulating many rates of deformation revealed an optimum rate of deformation that maximizes the length of nephron segments (Figure 7h). The computational model also predicted the experimentally observed radial distribution of nephron segments in encapsulated kidney organoids (Figure S23, Supporting Information). Finally, modifying cell–cell interactions in the model, which recapitulates cell extrusion from organoids in suspension culture, gave rise to the homogenous distribution of nephron segments observed in suspension culture (Figure S24, Supporting Information). Together, our experimental and computational data suggest that the extent of deformation of the hydrogel–organoid interface regulates the length and morphology of nephron segments in encapsulated kidney organoids.

3. Discussion

In this study, we encapsulated differentiating kidney organoids within viscoelastic alginate hydrogels in order to test the hypothesis that mechanical signals regulate nephrogenesis. Our data revealed that viscoelasticity of the encapsulating matrix modulates the spatial pattern of nephron segments in kidney organoids. 3D encapsulation also generated more convoluted tubular nephron segments as compared to suspension culture. Our computational model suggested that the extent of deformation of the hydrogel-organoid interface is a critical variable that regulates nephron length and morphology. Finally, elevated extracellular Ca^{2+} levels in the culture medium, which arise due to the loss of Ca^{2+} from alginate hydrogels, increased the fraction of tubular nephron segments in kidney organoids.

In contrast to Matrigel and type I collagen, alginate hydrogels supported kidney organoid differentiation without allowing significant cell migration from the organoid. Modifying the encapsulation timing or the hydrogel concentration may enable more consistent differentiation and reduce the cell migration observed in type I collagen and Matrigel hydrogels. Relative to alginate hydrogels used previously for kidney organoid culture, Ca^{2+} crosslinked alginate used here was considerably more viscoelastic and more closely approximated the viscoelastic properties of the embryonic mouse kidney (Table S2, Supporting Information). Moreover, the alginate used in the current study was not oxidized, enabling extended culture times as compared to prior studies that were limited to less than 1 week of encapsulated culture.[10] Finally, the syringe mixing protocol used here permitted the 3D encapsulation of organoids within the hydrogel as opposed to 2.5D systems where alginate hydrogels have been added on top of cells differentiated on transwell membranes.[10,11]

In hydrogels with slow rates of stress relaxation, nephron segments were located along the organoid perimeter, while segments were more broadly distributed throughout organoids encapsulated in hydrogels with fast relaxation. These observations are consistent with previous findings that viscoelasticity affects the spatial distribution of proliferating cells within epithelial spheroids.[14] Relative to suspension culture, the lack of nephron segments in the core of encapsulated organoids is likely due, in part, to oxygen diffusion limitations in alginate hydrogels[37] and the inability of encapsulated organoids to extrude dead cells throughout differentiation.

In contrast to viscoelasticity, stiffness did not significantly impact the distribution of nephron segments, nephron patterning, or nephron morphology. Stiffness also has been shown to not affect lumen formation for hPSCs encapsulated in alginate hydrogels.[38] However, in previous studies with kidney organoids, stiffness affected the transcriptional profile of podocytes,[9] the presence of proteins associated with fibrosis and epithelial–mesenchymal transition,[10] and the rate of differentiation.[7] The independence of stiffness and nephron distribution, patterning, and morphology in this study may be due to the limited stiffness range investigated, gradual softening of stiff alginate hydrogels after extended immersion in culture medium, the type and density of conjugated adhesion ligands, or the size of the kidney organoids encapsulated. While stiffness did not affect the aspects of nephrogenesis quantified in this study, it is likely that transcriptional differences result from changing matrix stiffness, as reported previously for kidney organoids.[9]

Proximal and distal tubule nephron segments were significantly more convoluted when kidney organoids were differentiated within alginate hydrogels. Relative to suspension culture and transwell culture,[39] the convoluted morphologies of tubular nephron segments in encapsulated organoids are more reminiscent of nephron morphology in vivo. Convoluted tubular segments were observed independent of stiffness, viscoelasticity,

© 2024 Wiley-VCH GmbH

15214095, 2024, 14, Downloaded from https://onlinelibrary.wiley.com/doi/10.1002/adma.202308325 by Seoul National University, Wiley Online Library on [14/05/2024]. See the Terms and Conditions (https://onlinelibrary.wiley.com/terms-and-conditions) on Wiley Online Library for rules of use; OA articles are governed by the applicable Creative Commons License

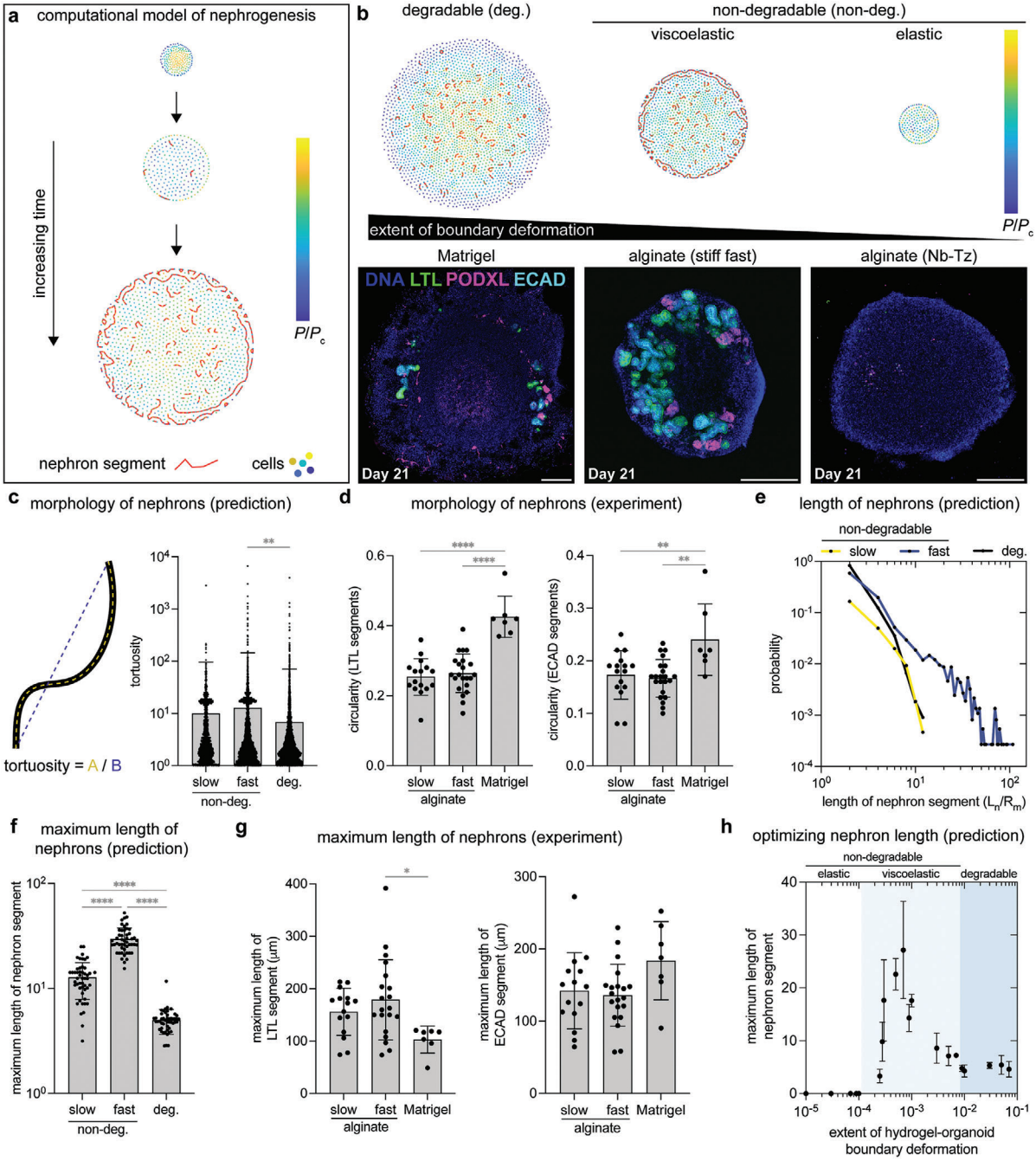


Figure 7. The extent of deformation of the hydrogel–organoid interface regulates the morphology and length of nephron segments. a) Representative simulations of nephrogenesis in kidney organoids. Color bar indicates the pressure (P) experienced by cells relative to a critical pressure (P_c). b) Representative simulations and fluorescent images of kidney organoids differentiated within hydrogels with different extents of deformation. Scale bars represent 200 μm. Alginate covalently crosslinked with Nb-Tz chemistry was used to approximate an elastic hydrogel. c) Tortuosity of nephron segments in simulated kidney organoids differentiated in degradable materials or nondegradable materials with slow and fast rates of boundary deformation. d) Circularity of nephron segments for kidney organoids differentiated in alginate or Matrigel hydrogels; Matrigel was used experimentally as a representative degradable material. The circularity values for alginate hydrogels were also reported in Figure 3g and are included here for comparison. Both soft and stiff alginate hydrogels are included in the quantification of fast and slow conditions. Predicted e) length distribution and f) maximum length of simulated nephron segments. L_n represents the length of a nephron segment and R_m is the radius of a cell (Table S1, Supporting Information). g) Maximum length of nephron segments for kidney organoids differentiated in alginate or Matrigel hydrogels. Both soft and stiff alginate hydrogels are included in the quantification of fast and slow conditions. h) Prediction of the simulated maximum length of nephron segments as a result of the hydrogel–organoid boundary deformation. Statistical comparisons were performed using an ordinary one-way ANOVA (c, d, f, and g). Data represent an average of 49 simulations (c, e, and f) or three simulations (h). $n = 2158$, 3704, and 5517 nephron segments per condition, respectively (c). $n = 15$, 20, and 7 organoids per condition (d) or 16, 22, and 7 organoids per condition (g). Data represent mean ± SD. $^*p \leq 0.05$, $^{**}p \leq 0.01$, and $^{****}p \leq 0.0001$.

© 2024 Wiley-VCH GmbH

15214095, 2024, 14, Downloaded from https://onlinelibrary.wiley.com/doi/10.1002/adma.202308325 by Seoul National University, Wiley Online Library on [14/05/2024]. See the Terms and Conditions (https://onlinelibrary.wiley.com/terms-and-conditions) on Wiley Online Library for rules of use; OA articles are governed by the applicable Creative Commons License

15214095, 2024, 14, Downloaded from https://onlinelibrary.wiley.com/doi/10.1002/adma.202308325 by Seoul National University, Wiley Online Library on [14/05/2024]. See the Terms and Conditions (https://onlinelibrary.wiley.com/terms-and-conditions) on Wiley Online Library for rules of use; OA articles are governed by the applicable Creative Commons License

or RGD peptide conjugation, which suggests that 3D confinement may be the important factor that results in convoluted tubule morphologies. These findings are consistent with previous reports that confinement of kidney organoids in soft dynamic hydrogels can influence the lumen morphology of proximal tubules.[10] Confinement may also drive differences in cell cycle progression,[12] differentiation,[40] and the transcriptomic profile[41] of kidney organoids. During embryonic kidney development, the renal capsule may confine the nephrogenic niche in a similar manner and impart mechanical signals, in addition to biochemical signals,[42] that contribute to the patterning and morphology of tubular nephron segments.

Our computational model predicted that the extent of deformation of the hydrogel–organoid interface regulates the length and morphology of nephron segments in differentiating kidney organoids. Our experimental data are consistent with this prediction apart from the length of distal nephron segments, which is independent of the mechanical properties of the encapsulating hydrogel. One possible explanation for this discrepancy between the computational prediction and experimental measurements could be related to the relative timing of differentiation of the proximal and distal nephron segments. Proximal segments appear earlier during differentiation[43] while distal tubule segments appear later when the hydrogel–organoid interface experiences smaller deformations. Moreover, Matrigel contains a complex mixture of proteins[22] that may impact the formation of nephron segments in a manner that is independent of matrix deformation. Finally, extension of the computational model to 3D may also resolve this difference. Consistent with previous literature,[10] our computational model and experimental data suggest that confinement in a rigid hydrogel with limited deformation can significantly reduce the formation of nephron segments. While simulations predicted that nondegradable viscoelastic matrices can deform in a manner that optimizes the length of nephron segments in kidney organoid culture, further investigation will be required to determine how the optimized nephron length compares to the physiological size of nephrons in the human kidney. In contrast to encapsulated organoids, accurately simulating nephron formation in suspension culture remains challenging due to the extrusion of cells that takes place throughout differentiation.

Increased levels of extracellular Ca^{2+} in the culture medium during kidney organoid differentiation decreased the ratio of glomerulus-to-tubule nephron segments. The resulting tubule-rich kidney organoids contained nephron segments where ≈65% of the segment area corresponded to tubule cells (LTL and ECAD) and ≈35% corresponded to podocytes (PODXL). Relative to hESC-derived kidney organoids generated[44] using the Takasato protocol,[4] we observed a higher ratio of podocytes/tubule cells in our tubule-rich kidney organoids, which is likely related to the significantly higher levels of FGF9 (200 ng mL^{-1}) used in the Takasato protocol.

Our data suggest a possible role for extracellular Ca^{2+} in specifying nephron patterning during kidney development. Similar decreases in the ratio of glomerulus-to-tubule nephron segments have been reported in response to prolonged canonical Wnt signaling in kidney organoids[45] and embryonic kidneys[46] in culture. In addition, the noncanonical Ca^{2+}/NFAT Wnt signaling pathway has been implicated in the early stages of nephrogenesis.[47] Extracellular Ca^{2+} levels may therefore impact nephron patterning through Wnt signaling. Moreover, treatment of kidney organoids with K252a, which inhibits Ca^{2+}/calmodulin-dependent kinase II, increases the fraction of tubular cells from 35.2% to 70.4% in kidney organoids.[44] These data further suggest an important relationship between Ca^{2+} and nephron pattering. In embryonic kidneys, the glomerulus-to-tubule ratio of nephron segments is affected by signaling from the renal stroma.[48] Thus, extracellular Ca^{2+} may also indirectly affect nephron patterning in kidney organoids by altering the stromal population of the organoid. Further investigation will be required to understand the signaling pathways that drive changes in nephron patterning observed in this study and to understand how the timing and extent of elevated Ca^{2+} levels affect kidney organoid differentiation. Our data suggest that elevated Ca^{2+} exposure largely occurs during the first 2 d after encapsulation when cells are transitioning through the metanephric mesenchyme stage of differentiation. However, we also observe that prolonged exposure to elevated Ca^{2+} during suspension culture reproduces the same nephron patterning shift observed in encapsulated organoids. The similar patterning shift observed, independent of the exact timing of Ca^{2+} elevation, suggests varying levels of sensitivity to extracellular Ca^{2+} exposure throughout kidney organoid differentiation.

In conclusion, this study reveals that mechanical and soluble signals derived from 3D encapsulation in alginate hydrogels regulate nephron patterning and morphology in kidney organoids. These findings demonstrate that the 3D mechanical microenvironment is an important consideration for kidney regenerative medicine and suggest that the extent of cell-induced deformation of hydrogels broadly regulates epithelial morphogenesis during 3D culture of organoids. While encapsulation in hydrogels with mechanical properties that vary around the properties of the embryonic mouse kidney significantly impacted nephrogenesis, it remains unclear if the developing mouse kidney accurately approximates the mechanical environment in the developing human kidney. These data motivate further investigation into the physiological relevance of the 3D mechanical environment in terms of kidney organoid maturation, function, and integration in vivo. In terms of scaffold design, there remains an unmet need to design hydrogel scaffolds that recapitulate the mechanical properties of developing tissues.

4. Experimental Section

Mouse Tissue: Mouse embryonic kidney tissue was obtained from mice that were handled according to the guidelines of the Institutional Animal Care and Use Committee at Boston Children's Hospital (Laboratory of Jordan A. Kreidberg).

Maintenance of Human Pluripotent Stem Cells: H9 (WiCell) hESCs and WTC11 hRETtdTomato:GCaMP6f human induced pluripotent stem cells (Jain Lab, WUSTL, The (Re)Building a Kidney Consortium[49–51]) were cultured in mTeSR1 feeder-free medium (85857, Stemcell Technologies, Seattle, WA). Cells were maintained in six-well tissue culture plates (353046, Corning) coated with hESC-qualified Matrigel (354277, Corning). Medium changes were performed daily, and the incubator was maintained at 37 °C and 5% CO_2. Cells were passaged as aggregates using ReLeSR (05872, Stemcell Technologies) every 3 d using a 1:3 to 1:5 split ratio. Cells were cryopreserved using mFreSR (05855, Stemcell Technologies). Mycoplasma testing was conducted using a MycoFluor mycoplasma detection kit (M7006, Invitrogen). Markers for stem cell

 © 2024 Wiley-VCH GmbH

pluripotency were evaluated using an immunocytochemistry kit for SOX2, OCT-3/4, and NANOG (SC021, R&D Systems). Protocols for working with hESCs were approved by the Harvard University Embryonic Stem Cell Research Oversight Committee.

3D Kidney Organoid Differentiation: After thawing, hPSCs (H9) were passaged at least twice and grown to ≈90% confluency before starting the kidney organoid differentiation protocol. On day −2, cells were washed twice with 1 × D-PBS (no Ca^{2+} or Mg^{2+}, 37354, Stemcell Technologies). Cells were next incubated in 500 µL ACCUTASE (07920, Stemcell Technologies) for 8 min at 37 °C and 5% CO_2 and resuspended at a concentration of 500 000 cells mL^{-1} in mTeSR1 supplemented with 10×10^{-6} M Y-27632 dihydrochloride (1254, Tocris Bioscience). 200 µL of cell suspension was added per well of ultra-low attachment round bottom 96-well microplate (7007, Corning). On day −1, medium in each well was replaced with mTeSR1 (without Y-27632 dihydrochloride). On day 0, medium was replaced with advanced minimum essential medium (AMEM) (12492013, Thermo Fisher Scientific) supplemented with 6×10^{-6} M CHIR 99021 (4423, Tocris Bioscience) and 2×10^{-3} M GlutaMAX (35050061, Thermo Fisher Scientific). On days 2 and 4, medium was replaced with AMEM supplemented with 6×10^{-6} M CHIR 99021 and 2×10^{-3} M GlutaMAX. On day 5, medium was replaced with AMEM supplemented with 2×10^{-3} M GlutaMAX. On days 7 and 9, medium was replaced with AMEM supplemented with 3×10^{-6} M CHIR 99021, 10 ng mL^{-1} recombinant human FGF9 (273-F9-025/CF, R&D Systems), and 2×10^{-3} M GlutaMAX. On days 12 and 15, medium was replaced with AMEM supplemented with 10 ng mL^{-1} FGF9 and 2×10^{-3} M GlutaMAX. On day 18, medium was replaced with AMEM supplemented with 2×10^{-3} M GlutaMAX. On day 21, kidney organoids were collected. Cells were maintained at 37 °C and 5% CO_2 throughout the differentiation protocol. A medium volume of 200 µL/well was used throughout the differentiation protocol.

Alginate Hydrogel Preparation: Experiments were conducted with sodium alginate (Protanal LF10/60; FMC) with an average molecular weight (MW) of ≈135 kDa and 25%–35% β-D-mannuronic acid and 65%–75% α-L-guluronic acid monomers. Irradiation with a 3mRad cobalt source was used to modify the average MW of alginate to ≈44 kDa. RGD functionalization of alginate was performed using aqueous carbodiimide chemistry[52] as described previously.[53] Briefly, alginate functionalization was conducted with a 1% solution of sodium alginate in 0.1 M MES buffer [0.1 M MES hydrate (M8250, Sigma-Aldrich) + 0.3 M sodium chloride (S9888, Sigma-Aldrich)] using empirically determined reaction conditions.[53] *N*-(3-Dimethylaminopropyl)-*N*′-ethylcarbodiimide hydrochloride (EDC, E1769, Sigma-Aldrich) and *N*-hydroxysulfosuccinimide (sulfo-NHS, 24510 Thermo Fisher Scientific) were used to link a linear RGD peptide (GGGGRGDSP; Peptide 2.0) to the carboxylate moieties on the alginate backbone. The reaction was performed at room temperature for 20 h and quenched with 125 mg hydroxylamine hydrochloride (159417, Sigma-Aldrich)/g alginate. High MW alginate was functionalized with a degree of substitution (DS) of 20, which corresponds to 166.67×10^{-6} M RGD per gram of alginate. Low MW alginate was functionalized using the same molar concentrations of reactants. Functionalized alginate was dialyzed (MW cutoff 3.5 kDa, 132594, Spectra/Por 6; Repligen) for 3 d in decreasing NaCl solutions in DI water (starting at 0.13 M NaCl). After dialysis, alginate was treated with 0.5 g of activated charcoal (C9157, Sigma-Aldrich)/g alginate for 30 min with continuous stirring. Finally, alginate was sterile-filtered (0.22 µm), lyophilized, and stored at −20 °C. Nb- and Tz-functionalized alginates (≈275 kDa) were functionalized with a DS of 5 as described previously.[54] Unless stated otherwise, all alginate hydrogels had a final alginate concentration of 20 mg mL^{-1} and were functionalized with RGD peptide as described above.

Gel Permeation Chromatography: The molar mass distribution of high- and low-MW alginate (Table S3, Supporting Information) was determined using a 1260 Infinity II gel permeation chromatography/size exclusion chromatography system (Agilent Technologies) at 40 °C. The system was equipped with a multi-angle light scattering and refractive index detector. Prior to analysis, lyophilized alginate was dissolved in DMEM/F-12 (11320033, Thermo Fisher Scientific) medium at a concentration of 25 mg mL^{-1}, diluted to a concentration of 2.5 mg mL^{-1} in 100×10^{-3} M $NaNO_3$ with 5% w/v sodium azide, and filtered through a nylon filter (0.2 µm). 100 µL sample injections were performed using a tandem column, which included a Tosoh G4000PWxl 7.8 mm ID × 30 cm and Tosoh G5000PWxl 7.8 mm ID × 30 cm, eluting with 0.5 mL min^{-1} of 100×10^{-3} M $NaNO_3$ with 5% w/v sodium azide mobile phase at 40 °C. System calibration was performed with a narrow standard of polyethylene oxide.

Cell Encapsulation: Kidney organoids were encapsulated in alginate hydrogels on day 0 or day 7 of the differentiation protocol using 1 mL Luer-Lok syringes (309628, BD) and a female Luer thread style coupler. Alginate was dissolved in DMEM/F-12 (11320033, Thermo Fisher Scientific) medium and combined with kidney organoids in one syringe. In another syringe, calcium sulfate dihydrate (C3771, Sigma-Aldrich) was combined with cell culture medium. The contents of the syringes were mixed (6–8 times) and deposited between glass plates to generate 2-mm-thick gels. Alginate was incubated at 37 °C and 5% CO_2 for 1 h and then transferred to a non-TC treated 12-well plate with 1.2 mL of medium. For non-RGD functionalized alginate hydrogels, alginate was cast onto glass, organoids were deposited on top immediately after casting, and then another layer of alginate was added on top to fully encapsulate the organoids. Encapsulation using Nb-Tz alginate hydrogels[54] was performed using the same method as RGD alginate. Encapsulation in rat tail type I collagen (354249, Corning), low-concentration Matrigel (356231, Corning), or high-concentration Matrigel (354248, Corning) was completed by mixing pre-gel with organoids with a wide bore pipette and casting directly onto a non-TC treated 12-well plate, incubating at 37 °C and 5% CO_2 for 1 h, and then immersing in culture medium.

Cryosectioning: Kidney organoids were rinsed in PBS (46-013-CM, Corning), fixed in 4% paraformaldehyde (15710, Electron Microscopy Sciences) for 1 h at room temperature, and washed three times with PBS. After washing, organoids were immersed in 30% sucrose (S0389, Sigma-Aldrich) in PBS overnight (>12 h) at 4 °C. Next, organoids were embedded in Tissue-Tek O.C.T. compound (4583, Sakura), frozen on dry ice, and immediately cryosectioned or stored at −80 °C. 15 or 50-µm-thick sections were cut throughout the entire height of the organoid using a cryostat (CM 1950, Leica) at a temperature of ≈−18 °C. Sections were placed on Superfrost Plus microscope slides (95057-985, VWR) and stored at −80 °C until immunofluorescence staining.

Kidney Organoid Staining: To label nephron segments, sectioned kidney organoids were thawed at room temperature and allowed to dry for ≈30 min. O.C.T. compound was removed by washing the sections three times for 10 min with PBS. Next, sections were immersed in blocking buffer containing 5% (w/v) donkey serum (ab7475, Abcam) in 0.3% PBST at room temperature for 1 h. After blocking, samples were washed three times with PBST and then blocked with the streptavidin biotin blocking kit (SP-2002, Vector Laboratories). Samples were immersed in streptavidin for 15 min, washed with PBS three times, immersed in biotin for 15 min and washed with PBS. Samples were then immersed in primary antibodies overnight at 4 °C. Samples were then placed at room temperature for 15 min and washed three times with PBS. Next, samples were immersed in secondary antibody solution for 1 h at room temperature. To prepare samples for microscopy, 75 µL of Fluoromount-G mounting medium (35050061, Thermo Fisher Scientific) were added and samples were sealed with a no. 1.5 glass coverslip (48393-241, VWR) and CoverGrip coverslip sealant (23005, Biotium). A complete list of reagents used for staining kidney organoids is provided in Table S4 (Supporting Information).

Transmission Electron Microscopy: Kidney organoids were fixed at 4 °C for ≈72 h in a 0.1 M sodium cacodylate buffer containing 2.5% glutaraldehyde and 2.5% paraformaldehyde. Organoids were postfixed with 1% osmium tetroxide and 1.5% potassium ferrocyanide for 1 h. Samples were then washed twice in water and once in 50×10^{-3} M maleate buffer pH 5.15 (MB). Next, samples were incubated in 1% uranyl acetate in MB for 1 h. After incubation, samples were washed once in MB and twice in water. Samples were next dehydrated in a graded series of alcohols, transferred to propylene oxide, and infiltrated with a 1:1 mixture of propylene oxide and TAAB 812 Epon (TAAB Laboratories Equipment Ltd) for ≈24 h. Samples were then embedded in TAAB 812 Epon and polymerized at 60 °C for 48 h. Embedded samples were sectioned (50–80 nm) using a Reichert Ultracut-S microtome (Leica), mounted on copper

© 2024 Wiley-VCH GmbH

15214095, 2024, 14, Downloaded from https://onlinelibrary.wiley.com/doi/10.1002/adma.202308325 by Seoul National University, Wiley Online Library on [14/05/2024]. See the Terms and Conditions (https://onlinelibrary.wiley.com/terms-and-conditions) on Wiley Online Library for rules of use; OA articles are governed by the applicable Creative Commons License

grids, and stained with lead citrate. Images were acquired using a JEOL 1200EX transmission electron microscope (JEOL) and an AMT 2k CCD camera (Advanced Microscopy Techniques). Unless stated otherwise, all chemicals were purchased from Electron Microscopy Sciences.

Fluorescence Microscopy: Fluorescence microscopy was conducted using a Zeiss LSM 710 laser scanning confocal microscope and a 5× air objective or a 10×, 20×, or 40× water-immersion objective. The 405, 488, 594, and 647 nm channels were acquired sequentially. Unless stated otherwise, images in the manuscript represent single confocal slices of 50-µm-thick organoid cryosections.

Quantification of Nephron Segments: The area of nephron segments was quantified using ImageJ. Fluorescence images of organoids were converted to binary images. Total fluorescent area (*A*) and perimeter (*P*) for each nephron segment were quantified using the analyze particles command. The circularity (*C*) of nephron segments was calculated using Equation (1).

$$C = \frac{4\pi A}{P^2} \tag{1}$$

Atomic Force Microscopy: Experiments were conducted using a JPK NanoWizard 4XP BioAFM (Bruker) and a cylindrical tip AFM probe ($k \approx 0.235$ N m^{-1}) (SAA-SPH-10 µm, Bruker). Mouse embryonic kidneys (≈E15–E17) were dissected, embedded in agar (100262, MP Biomedicals), and cut into 200-µm-thick sections using a microtome (Leica VT1000 S). Tissue sections were stored in DMEM/F-12 (Thermo Fisher Scientific) at 4 °C until analysis, which was conducted within 48 h of sectioning. AFM measurements were conducted at room temperature (≈22 °C), and tissue sections remained immersed in DMEM/F-12 throughout the AFM measurements. The Young's modulus was measured over 25 µm^2 areas using quantitative imaging mode with a setpoint of 1.5 nN, *z* length of 1.5 µm, *z* speed of 78.12 µm s^{-1}, and pixel time of 48 ms. Stress relaxation measurements were conducted using contact mode force spectroscopy. To measure stress relaxation, the AFM probe was brought into contact with the tissue surface with a setpoint of 1 nN, *z* length of 1 µm, and *z* speed of 1 µm s^{-1}. Next, the probe underwent a step indentation into the tissue with a *z* length of 0.8 µm and *z* speed of 1 µm s^{-1}. The probe was held at constant height for 120 s while stress relaxation was recorded at a sample rate of 20 Hz.

Rheological Measurements: Experiments were conducted using a stress-controlled rheometer (Discovery HR-3, TA Instruments) and a 20-mm parallel-plate with a 900 µm gap. Alginate was mixed with calcium sulfate to initiate gelation and the top plate was immediately lowered. Extra material was trimmed, and 5 cSt silicone oil (317667, Sigma-Aldrich) was added to prevent evaporation. Alginate was allowed to gel until a stable modulus was reached (1 h). Shear storage and loss moduli were measured at 1% strain and 1 Hz. Stress relaxation tests were conducted for 3 h at 15% strain. All measurements were conducted at 37 °C.

Parallel-Plate Compression of Alginate Gels: Experiments were conducted using a parallel plate mechanical tester (model 3220-ES Series III, Bose) and a previously developed testing program to obtain stiffness and viscoelasticity.[55] Alginate hydrogels were cast to a thickness of 2 mm and diameter of ≈16 mm. After incubation at 37 °C for 1 h in a cell culture incubator, hydrogels were transferred to 12-well plates with 1.2 mL of culture medium per gel to be consistent with the cell culture experiments. Gels were incubated for a total of 15 d, and the culture medium was changed with the same frequency as that used for cell culture experiments. Mechanical analysis was conducted on days 0, 5, 10, and 15 to assess stability over the timescales relevant to organoid culture. For mechanical analysis, alginate hydrogels were loaded onto the bottom plate and 100 µL of culture medium was added on top of the sample to ensure that the hydrogel did not dehydrate during testing. ≈1 g of pre-loading was applied to samples prior to initiating the test. Next, 10% strain was applied in compression over 2 s followed by constant strain during a stress relaxation test for 300 s. All measurements were conducted at room temperature.

Quantification of Force/Stress Relaxation Time: The relaxation time of alginate hydrogels was quantified by calculating the $t_{1/3}$ relaxation time, which represents the time it takes for the hydrogel to dissipate 33% of the initial force or stress measured during the stress relaxation test (described above).

Calcium Concentration Assay: The free calcium ion concentration of culture medium was measured using a colorimetric calcium assay kit (ab102505, Abcam). Samples were analyzed using a multiplate reader (Synergy Neo2, BioTek).

Osmolality Adjustment and Measurements: The osmolality of cell culture medium was adjusted by adding various concentrations of unpolymerized alginate (MW ≈ 44 kDa) or D-mannitol (M4125, Sigma-Aldrich). Osmolality was measured using a vapor pressure osmometer (VAPRO model 5600, Wescor). Instrument calibration was performed using 100, 290, and 1000 mmol kg^{-1} osmolality standards (ELITechGroup).

Computational Model of Nephrogenesis: The computational model, inspired by previous work,[14,56–61] consists of a particle-based model wherein the particles are individual cells. In the computational model, cells have the following properties: a) physical intercellular interaction using short-range interaction, b) local pressure dictated self-propulsion, growth, and subsequent cell division resulting in identical daughter cells, and finally c) linkage formation between neighboring cells using local pressure and velocity information. These properties of the computational model are described in detail in the Supporting Information.

Statistical Analysis: Statistical analysis was performed using GraphPad Prism (9.4; GraphPad software). Unless stated otherwise, all experiments were conducted with a minimum of three independent replicates. For stem cell differentiations, independent replicates are defined as separate differentiations. Additional details about the specific statistical tests are included in the figure legends.

Supporting Information

Supporting Information is available from the Wiley Online Library or from the author.

Acknowledgements

The authors thank members of the Mooney Lab, Laurence Daheron, Yi Lin, Kyle McCracken, Mohammad Zarei, and Matthias Kollert for helpful discussions. The authors also thank Mary Taglienti for assistance with mouse embryonic kidney dissections, Nicholas Colella for assistance with AFM, Alexander Stafford for providing Nb- and Tz-functionalized alginate, the laboratory of Jordan A. Kreidberg for providing mouse embryos, and Haihui Joy Jiang, Khaled Abdelazim, and the laboratory of George M. Whitesides for assistance with osmolality measurements. Electron microscopy imaging, consultation and/or services were performed in the Harvard Medical School Electron Microscopy Facility. The use of WTC11 hRETtd-Tomato:GCaMP6f human induced pluripotent stem cells was made possible by support from the Kidney Translational Research Center (KTRC) and the ATLAS D2K (U24DK135157) and WU-PCEN (P50DK133943) grants. B.A.N. was supported by a NIH F32 postdoctoral fellowship (F32DK134115, UH3TR002155 and R37DK39773) and a NIH T32 postdoctoral fellowship (T32EB016652) from the Organ Design and Engineering Training Program. P.B. acknowledges funding by the Netherlands Organization for Scientific Research (NWO, Grant No. 17835). N.N.L. was supported by a NIH T32 fellowship (T32HL007609). J.V.B. was supported by NIH grants UH3 TR002155 and R37 DK39773. Work was performed in part at the Harvard University Center for Nanoscale Systems (CNS), which is a member of the National Nanotechnology Coordinated Infrastructure Network (NNCI) and was supported by the National Science Foundation under NSF Award No. ECCS-2025158. Additional support was provided by Harvard MRSEC (DMR-2011754) and the Wellcome Leap HOPE program.

Conflict of Interest

J.V.B. is an inventor on kidney organoid patents assigned to Mass General Brigham Healthcare.

© 2024 Wiley-VCH GmbH

15214095, 2024, 14, Downloaded from https://onlinelibrary.wiley.com/doi/10.1002/adma.202308325 by Seoul National University, Wiley Online Library on [14/05/2024]. See the Terms and Conditions (https://onlinelibrary.wiley.com/terms-and-conditions) on Wiley Online Library for rules of use; OA articles are governed by the applicable Creative Commons License

Data Availability Statement

The data that support the findings of this study are available from the corresponding author upon reasonable request.

Keywords

biomaterials, biomimetic scaffolds for tissue regeneration, directed differentiation of human pluripotent stem cells, extracellular matrices, mechanical confinement

Received: August 16, 2023
Revised: December 6, 2023
Published online: January 10, 2024

[1] R. Witzgall, D. Brown, C. Schwarz, J. V. Bonventre, *J. Clin. Invest.* **1994**, *93*, 2175.
[2] T. Kusaba, M. Lalli, R. Kramann, A. Kobayashi, B. D. Humphreys, *Proc. Natl. Acad. Sci. USA* **2014**, *111*, 1527.
[3] B. D. Humphreys, M. T. Valerius, A. Kobayashi, J. W. Mugford, S. Soeung, J. S. Duffield, A. P. Mcmahon, J. V. Bonventre, *Cell Stem Cell* **2008**, *2*, 284.
[4] M. Takasato, P. X. Er, H. S. Chiu, B. Maier, G. J. Baillie, C. Ferguson, R. G. Parton, E. J. Wolvetang, M. S. Roost, S. M. Chuva De Sousa Lopes, M. H. Little, *Nature* **2015**, *526*, 564.
[5] B. S. Freedman, C. R. Brooks, A. Q. Lam, H. Fu, R. Morizane, V. Agrawal, A. F. Saad, M. K. Li, M. R. Hughes, R. V. Werff, D. T. Peters, J. Lu, A. Baccei, A. M. Siedlecki, M. T. Valerius, K. Musunuru, K. M. Mcnagny, T. I. Steinman, J. Zhou, P. H. Lerou, J. V. Bonventre, *Nat. Commun.* **2015**, *6*, 8715.
[6] R. Morizane, A. Q. Lam, B. S. Freedman, S. Kishi, M. T. Valerius, J. V. Bonventre, *Nat. Biotechnol.* **2015**, *33*, 1193.
[7] E. Garreta, P. Prado, C. Tarantino, R. Oria, L. Fanlo, E. Martí, D. Zalvidea, X. Trepat, P. Roca-Cusachs, A. Gavaldà-Navarro, L. Cozzuto, J. M. Campistol, J. C. Izpisúa Belmonte, C. Hurtado Del Pozo, N. Montserrat, *Nat. Mater.* **2019**, *18*, 397.
[8] K. A. Homan, N. Gupta, K. T. Kroll, D. B. Kolesky, M. Skylar-Scott, T. Miyoshi, D. Mau, M. T. Valerius, T. Ferrante, J. V. Bonventre, J. A. Lewis, R. Morizane, *Nat. Methods* **2019**, *16*, 255.
[9] N. J. Treacy, S. Clerkin, J. L. Davis, C. Kennedy, A. F. Miller, A. Saiani, J. K. Wychowaniec, D. F. Brougham, J. Crean, *Bioact. Mater.* **2023**, *21*, 142.
[10] F. A. A. Ruiter, F. L. C. Morgan, N. Roumans, A. Schumacher, G. G. Slaats, L. Moroni, V. L. S. Lapointe, M. B. Baker, *Adv. Sci.* **2022**, *9*, 2200543.
[11] T. Geuens, F. A. A. Ruiter, A. Schumacher, F. L. C. Morgan, T. Rademakers, L. E. Wiersma, C. W. Van Den Berg, T. J. Rabelink, M. B. Baker, V. L. S. Lapointe, *Biomaterials* **2021**, *275*, 120976.
[12] S. Nam, V. K. Gupta, H.-P. Lee, J. Y. Lee, K. M. Wisdom, S. Varma, E. M. Flaum, C. Davis, R. B. West, O. Chaudhuri, *Sci. Adv.* **2019**, *5*, eaaw6171.
[13] O. Chaudhuri, L. Gu, D. Klumpers, M. Darnell, S. A. Bencherif, J. C. Weaver, N. Huebsch, H.-P. Lee, E. Lippens, G. N. Duda, D. J. Mooney, *Nat. Mater.* **2016**, *15*, 326.
[14] A. Elosegui-Artola, A. Gupta, A. J. Najibi, B. R. Seo, R. Garry, C. M. Tringides, I. De Lázaro, M. Darnell, W. Gu, Q. Zhou, D. A. Weitz, L. Mahadevan, D. J. Mooney, *Nat. Mater.* **2023**, *22*, 117.
[15] B. M. Baker, C. S. Chen, *J. Cell Sci.* **2012**, *125*, 3015.
[16] H. Liu, K. Roy, *Tissue Eng.* **2005**, *11*, 319.
[17] S. Levenberg, N. F. Huang, E. Lavik, A. B. Rogers, J. Itskovitz-Eldor, R. Langer, *Proc. Natl. Acad. Sci. USA* **2003**, *100*, 12741.
[18] O. F. P. Santos, S. K. Nigam, *Dev. Biol.* **1993**, *160*, 293.
[19] R. Kher, E. C. Sha, M. R. Escobar, E. M. Andreoli, P. Wang, W. M. Xu, A. Wandinger-Ness, R. L. Bacallao, *Am. J. Physiol.: Cell Physiol.* **2011**, *301*, C99.
[20] H. J. Han, W. J. Sigurdson, P. A. Nickerson, M. Taub, *J. Cell Sci.* **2004**, *117*, 1821.
[21] M. Shi, K. W. Mccracken, A. B. Patel, W. Zhang, L. Ester, M. T. Valerius, J. V. Bonventre, *Nat. Biotechnol.* **2023**, *41*, 252.
[22] C. S. Hughes, L. M. Postovit, G. A. Lajoie, *Proteomics* **2010**, *10*, 1886.
[23] I.-M. Chung, N. O. Enemchukwu, S. D. Khaja, N. Murthy, A. Mantalaris, A. J. García, *Biomaterials* **2008**, *29*, 2637.
[24] H. M. Weber, M. V. Tsurkan, V. Magno, U. Freudenberg, C. Werner, *Acta Biomater.* **2017**, *57*, 59.
[25] N. O. Enemchukwu, R. Cruz-Acuña, T. Bongiorno, C. T. Johnson, J. R. García, T. Sulchek, A. J. García, *J. Cell Biol.* **2015**, *212*, 113.
[26] O. Chaudhuri, L. Gu, M. Darnell, D. Klumpers, S. A. Bencherif, J. C. Weaver, N. Huebsch, D. J. Mooney, *Nat. Commun.* **2015**, *6*, 6365.
[27] A. Chrisnandy, D. Blondel, S. Rezakhani, N. Broguiere, M. P. Lutolf, *Nat. Mater.* **2022**, *21*, 479.
[28] S. Nasseri, L. E. Bilston, N. Phan-Thien, *Rheol. Acta* **2002**, *41*, 180.
[29] J. W. Kim, S. A. Nam, J. Yi, J. Y. Kim, J. Y. Lee, S.-Y. Park, T. Sen, Y.-M. Choi, J. Y. Lee, H. L. Kim, H. W. Kim, J. Park, D.-W. Cho, Y. K. Kim, *Adv. Sci.* **2022**, *9*, 2103526.
[30] K. Y. Lee, D. J. Mooney, *Prog. Polym. Sci.* **2012**, *37*, 106.
[31] A. Kobayashi, M. T. Valerius, J. W. Mugford, T. J. Carroll, M. Self, G. Oliver, A. P. Mcmahon, *Cell Stem Cell* **2008**, *3*, 169.
[32] I. V. Grigorieva, A. Oszwald, E. F. Grigorieva, H. Schachner, B. Neudert, T. Ostendorf, J. Floege, M. T. Lindenmeyer, C. D. Cohen, U. Panzer, C. Aigner, A. Schmidt, F. Grosveld, R. V. Thakker, A. J. Rees, R. Kain, *J. Am. Soc. Nephrol.* **2019**, *30*, 1641.
[33] H. G. Rennke, B. M. Denker, *Renal Pathophysiology: The Essentials*, Wolters Kluwer, Philadelphia **2020**.
[34] M. Aragona, T. Panciera, A. Manfrin, S. Giulitti, F. Michielin, N. Elvassore, S. Dupont, S. Piccolo, *Cell* **2013**, *154*, 1047.
[35] M. A. Leroux, F. Guilak, L. A. Setton, *J. Biomed. Mater. Res.* **1999**, *47*, 46.
[36] B. Phipson, P. X. Er, A. N. Combes, T. A. Forbes, S. E. Howden, L. Zappia, H.-J. Yen, K. T. Lawlor, L. J. Hale, J. Sun, E. Wolvetang, M. Takasato, A. Oshlack, M. H. Little, *Nat. Methods* **2019**, *16*, 79.
[37] H. Hiemstra, L. Dijkhuizen, W. Harder, *Eur. J. Appl. Microbiol. Biotechnol.* **1983**, *18*, 189.
[38] D. Indana, P. Agarwal, N. Bhutani, O. Chaudhuri, *Adv. Mater.* **2021**, *33*, 2101966.
[39] J. M. Vanslambrouck, S. B. Wilson, K. S. Tan, E. Groenewegen, R. Rudraraju, J. Neil, K. T. Lawlor, S. Mah, M. Scurr, S. E. Howden, K. Subbarao, M. H. Little, *Nat. Commun.* **2022**, *13*, 5943.
[40] P. Hoang, A. Kowalczewski, S. Sun, T. S. Winston, A. M. Archilla, S. M. Lemus, A. G. Ercan-Sencicek, A. R. Gupta, W. Liu, M. I. Kontaridis, J. D. Amack, Z. Ma, *Stem Cell Rep.* **2021**, *16*, 1228.
[41] D. Sen, A. Voulgaropoulos, A. J. Keung, *BMC Biotechnol.* **2021**, *21*, 59.
[42] R. S. Levinson, E. Batourina, C. Choi, M. Vorontchikhina, J. Kitajewski, C. L. Mendelsohn, *Development* **2005**, *132*, 529.
[43] L. Saxén, *Organogenesis of the Kidney*, Cambridge University Press, Cambridge **1987**.
[44] H. Wu, K. Uchimura, E. L. Donnelly, Y. Kirita, S. A. Morris, B. D. Humphreys, *Cell Stem Cell* **2018**, *23*, 869.
[45] J. H. Low, P. Li, E. G. Y. Chew, B. Zhou, K. Suzuki, T. Zhang, M. M. Lian, M. Liu, E. Aizawa, C. Rodriguez Esteban, K. S. M. Yong, Q. Chen, J. M. Campistol, M. Fang, C. C. Khor, J. N. Foo, J. C. I. Belmonte, Y. Xia Belmonte, Y. Xia, *Cell Stem Cell* **2019**, *25*, 373.
[46] N. O. Lindström, M. L. Lawrence, S. F. Burn, J. A. Johansson, E. R. Bakker, R. A. Ridgway, C.-H. Chang, M. J. Karolak, L. Oxburgh, D. J. Headon, O. J. Sansom, R. Smits, J. A. Davies, P. Hohenstein, *Elife* **2015**, *4*, 04000.

© 2024 Wiley-VCH GmbH

15214095, 2024, 14, Downloaded from https://onlinelibrary.wiley.com/doi/10.1002/adma.202308325 by Seoul National University, Wiley Online Library on [14/05/2024]. See the Terms and Conditions (https://onlinelibrary.wiley.com/terms-and-conditions) on Wiley Online Library for rules of use; OA articles are governed by the applicable Creative Commons License

[47] S. F. Burn, A. Webb, R. L. Berry, J. A. Davies, A. Ferrer-Vaquer, A. K. Hadjantonakis, N. D. Hastie, P. Hohenstein, *Dev. Biol.* **2011**, *352*, 288.
[48] J. Yang, A. Blum, T. Novak, R. Levinson, E. Lai, J. Barasch, *Dev. Biol.* **2002**, *246*, 296.
[49] L. Oxburgh, T. J. Carroll, O. Cleaver, D. R. Gossett, D. K. Hoshizaki, J. A. Hubbell, B. D. Humphreys, S. Jain, J. Jensen, D. L. Kaplan, C. Kesselman, C. J. Ketchum, M. H. Little, A. P. McMahon, S. J. Shankland, J. R. Spence, M. T. Valerius, J. A. Wertheim, O. Wessely, Y. Zheng, I. A. Drummond, *J. Am. Soc. Nephrol.* **2017**, *28*, 1370.
[50] N. Tabibzadeh, L. M. Satlin, S. Jain, R. Morizane, *Am. J. Physiol.: Renal Physiol.* **2023**, *325*, F695.
[51] S. E. Howden, S. B. Wilson, E. Groenewegen, L. Starks, T. A. Forbes, K. S. Tan, J. M. Vanslambrouck, E. M. Holloway, Y.-H. Chen, S. Jain, J. R. Spence, M. H. Little, *Cell Stem Cell* **2021**, *28*, 671.
[52] D. G. Hoare, D. E. Koshland, *J. Am. Chem. Soc.* **1966**, *88*, 2057.
[53] J. A. Rowley, G. Madlambayan, D. J. Mooney, *Biomaterials* **1999**, *20*, 45.
[54] R. M. Desai, S. T. Koshy, S. A. Hilderbrand, D. J. Mooney, N. S. Joshi, *Biomaterials* **2015**, *50*, 30.
[55] B. R. Freedman, A. Kuttler, N. Beckmann, S. Nam, D. Kent, M. Schuleit, F. Ramazani, N. Accart, A. Rock, J. Li, M. Kurz, A. Fisch, T. Ullrich, M. W. Hast, Y. Tinguely, E. Weber, D. J. Mooney, *Nat. Biomed. Eng.* **2022**, *6*, 1167.
[56] A. N. Malmi-Kakkada, X. Li, H. S. Samanta, S. Sinha, D. Thirumalai, *Phys. Rev. X* **2018**, *8*, 021025.
[57] S. Sinha, A. N. Malmi-Kakkada, X. Li, H. S. Samanta, D. Thirumalai, *Soft Matter* **2020**, *16*, 5294.
[58] S. Sinha, X. Li, R. Das, D. Thirumalai, *J. Chem. Phys.* **2022**, *156*, 245101.
[59] D. Drasdo, S. Höhme, *Phys. Biol.* **2005**, *2*, 133.
[60] G. Schaller, M. Meyer-Hermann, *Phys. Rev. E* **2005**, *71*, 051910.
[61] D. A. Matoz-Fernandez, K. Martens, R. Sknepnek, J. L. Barrat, S. Henkes, *Soft Matter* **2017**, *13*, 3205.

© 2024 Wiley-VCH GmbH

15214095, 2024, 14, Downloaded from https://onlinelibrary.wiley.com/doi/10.1002/adma.202308325 by Seoul National University, Wiley Online Library on [14/05/2024]. See the Terms and Conditions (https://onlinelibrary.wiley.com/terms-and-conditions) on Wiley Online Library for rules of use; OA articles are governed by the applicable Creative Commons License